iScience

CellPress

Article

Intensified Ethylene Production via Chemical Looping through an Exergetically Efficient Redox Scheme

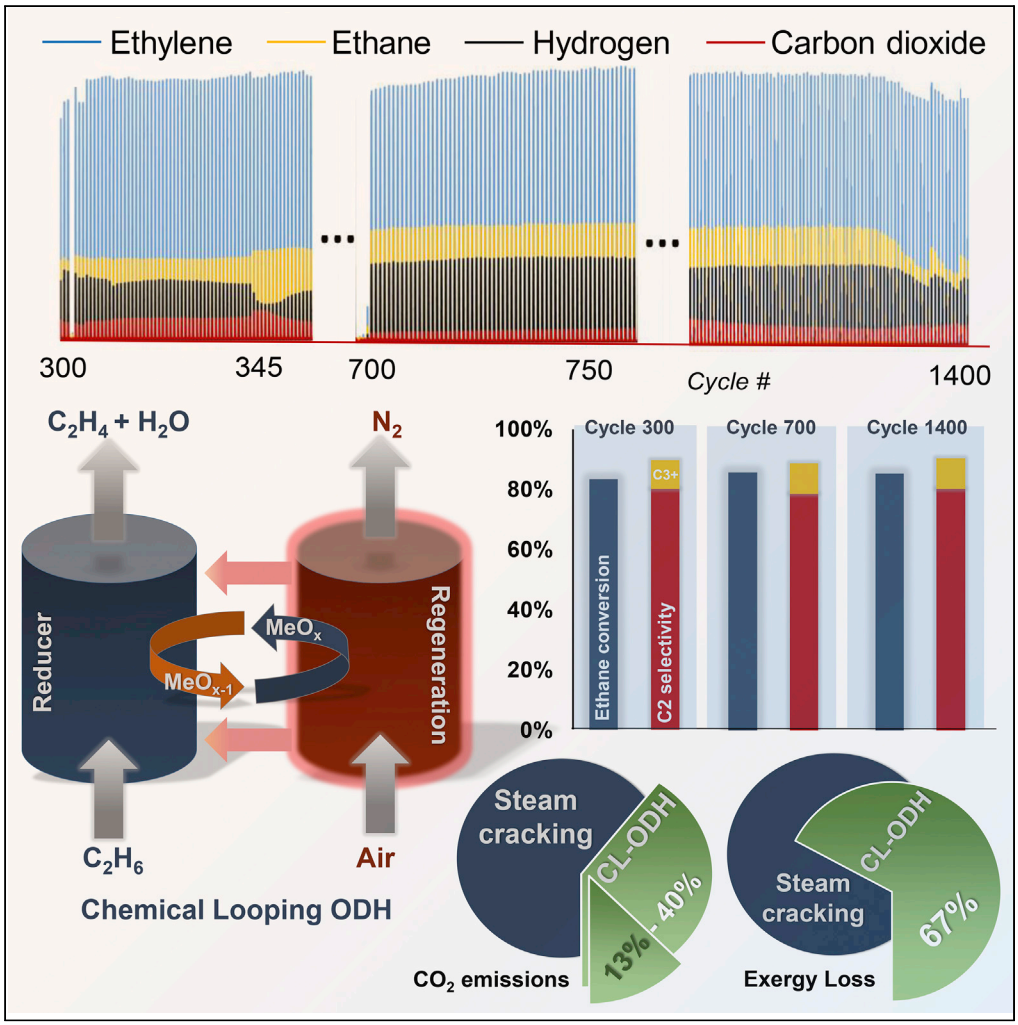

Luke M. Neal, Vasudev Pralhad Haribal, Fanxing Li

fli5@ncsu.edu

HIGHLIGHTS

Chemical-looping oxidative dehydrogenation intensifies ethylene production

Detailed process analysis shows ~87% emission reduction versus steam cracking

Reduction in exergy losses leads to substantial energy savings

Superior performance of a robust redox catalyst is demonstrated

Neal et al., iScience 19, 894–904
September 27, 2019
https://doi.org/10.1016/j.isci.2019.08.039

iScience

CellPress

Article

Intensified Ethylene Production via Chemical Looping through an Exergetically Efficient Redox Scheme

Luke M. Neal,[1,2] Vasudev Pralhad Haribal,[1,2] and Fanxing Li[1,3,*]

SUMMARY

Ethylene production via steam cracking of ethane and naphtha is one of the most energy and emission-intensive processes in the chemical industry. High operating temperatures, significant reaction endothermicity, and complex separations create hefty energy demands and result in substantial CO_2 and NO_x emissions. Meanwhile, decades of optimization have led to a thermally efficient, near-"perfect" process with ~95% first law energy efficiency, leaving little room for further reduction in energy consumption and CO_2 emissions. In this study, we demonstrate a transformational chemical looping–oxidative dehydrogenation (CL-ODH) process that offers 60%–87% emission reduction through exergy optimization. Through detailed exergy analyses, we show that CL-ODH leads to exergy savings of up to 58% in the upstream reactors and 26% in downstream separations. The feasibility of CL-ODH is supported by a robust redox catalyst that demonstrates stable activity and selectivity for over 1,400 redox cycles in a laboratory-scale fluidized bed reactor.

INTRODUCTION

Carbon capture and utilization has received significant attention for reducing anthropogenic emissions (E. Boot-Handford et al., 2014; Figueroa et al., 2008; Li et al., 2013; Tola and Pettinau, 2014; Volkart et al., 2013). However, most research activities in this area have focused on reducing CO_2 emissions from power and heat generation. This is understandable, since this sector alone accounts for approximately 31% of the 32 billion tons (CO_2 equivalent/year) of greenhouse gases emitted worldwide (Global Emissions, 2017). Meanwhile, the manufacturing sector, contributing 21% of the global greenhouse gas emissions (Friedrich, 2019), is often overlooked. For example, ethylene production via steam cracking releases over 1 ton of CO_2 per ton of olefin produced (Tao Ren, 2006). With a worldwide demand in excess of 150 million tons/year (Ethylene Global Supply Demand Analytics Service, 2018), ethylene production is one of the largest contributors to greenhouse gas emission in the manufacturing sector. Despite the high energy and carbon intensities associated with steam cracking, the operation is widely believed to be near optimal considering the continued research and improvements on the technology over the past 80+ years (Andrews and Pollock, 1959; Brown et al., 1983; Griffin and Moon, 1964; Heynderickx et al., 2001; Ludwig, 1951; Masaaki and Masaaki, 1967; Plehiers et al., 1990; Ranjan et al., 2012; Ruckaert et al., 1978; Sato and Ohnishi, 1971; W, 1963). Thermal efficiencies of up to 95% have been achieved through optimized furnace design and heat/steam integration (Zimmermann and Walzl, 2000). Although conventional wisdom would have indicated little room for further efficiency improvements in ethylene production, we recently reported a chemical looping–oxidative dehydrogenation (CL-ODH) scheme showing the potential to significantly reduce the energy consumption and CO_2 emissions compared with steam cracking (Haribal et al., 2017). In CL-ODH, as the name suggests, ethane is oxidatively dehydrogenated to ethylene and water, using the lattice oxygen of a chemical looping catalyst (reduction of the catalyst via Reaction 1a). Regeneration of this catalyst in air (Reaction 1b) provides the heat for ethylene formation.

CL-ODH (Reduction)

$$C_2H_6 + Me_yO_x \rightarrow C_2H_4 + H_2O + Me_yO_{x-1} \quad \text{(Reaction 1a)}$$

CL-ODH (Regeneration)

$$Me_yO_{x-1} + {}^1/_2 \cdot O_2 \rightarrow Me_yO_x \quad \text{(Reaction 1b)}$$

[1]Department of Chemical and Biomolecular Engineering, North Carolina State University, Raleigh, NC, USA

[2]These authors contributed equally

[3]Lead Contact

*Correspondence: fli5@ncsu.edu

https://doi.org/10.1016/j.isci.2019.08.039

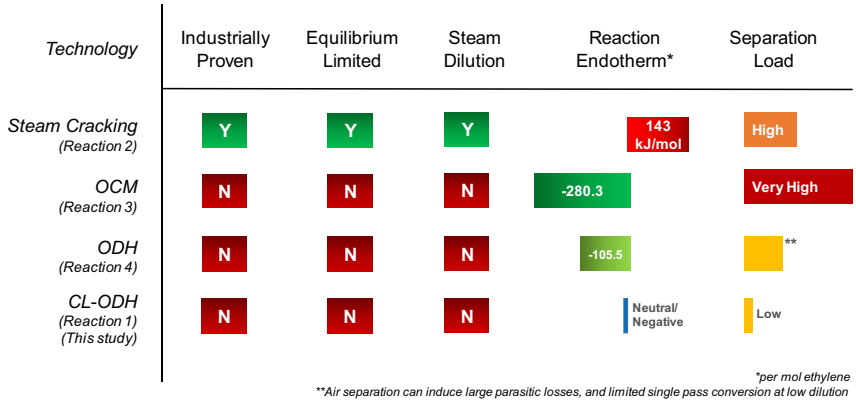

Figure 1. Comparison of Ethylene Production Techniques (Y Is Yes and N Is No)

In this study, using comprehensive second law analysis in conjunction with process models, we show the potential of CL-ODH to intensify the production of ethylene from ethane. It offers comprehensive proof-of-concept for CL-ODH (Haribal et al., 2017; Li and Neal, 2017; Neal et al., 2016; Sofranko et al., 2016; Yusuf et al., 2017), based on recent breakthroughs in redox catalyst development and process intensification. A net fuel demand reduction of up to 81% can be attained, leading to corresponding CO_2 emission savings. The near order-of-magnitude reduction in energy consumption and emissions confirmed in this work primarily results from the curtailed external fuel demand facilitated by the intrinsic advantages of CL-ODH in terms of (1) superior olefin yield, (2) removal of hydrogen (as water) before compression and refrigeration, (3) avoidance of steam usage, (4) significantly lowered operating temperature, and (5) advanced energy integration scheme. On a global scale, with the potential for saving >3 quadrillion BTU and cutting back over 100 million tons of CO_2 each year, the CL-ODH approach warrants further investigations as one of the potential "wedges" leading to a more carbon-neutral society (Socolow and Pacala, 2006). We also report a robust and highly selective prototype redox catalyst, which demonstrates exceptional performance, stability, and fluidization properties, that is significantly better than our previously reported Mg_6MnO_8 model catalyst system (Neal et al., 2016; Yusuf et al., 2017). High ethane conversion and ethylene selectivity were obtained over 1,400+ redox cycles in a laboratory-scale fluidized bed reactor. Performance data of this prototype redox catalyst confirms the potential of CL-ODH for appreciable exergy savings in both the upstream reaction section (up to 3.26 GJ/ton HVP or High Value Products, accounting for the produced C_2 and higher olefins), and downstream separation section (up to 0.89 GJ/ton HVP).

RESULTS AND DISCUSSION

The CL-ODH Approach to Ethylene Production

The need for transformative approaches to optimize ethylene production is well recognized and extensively investigated. Although the thermodynamic first law efficiency of conventional steam cracking is as high as ~95% (Zimmermann and Walzl, 2000), our second law analysis in the present study indicates a significant exergy loss, due to fuel combustion (cracking furnaces) and low energy quality from heat recovery. The downstream compression and cryogenic separation in conventional cracking leads to additional exergy losses. Pushing the cracking units to higher per-pass ethane conversions could reduce compression/separation loads. However, this is not practical owing to reaction equilibrium limitations (Reaction 2) and the propensity of ethylene to undergo secondary reactions, which eventually forms coke on the inner surfaces of cracking tubes.

Ethane cracking/pyrolysis

$$C_2H_6 \leftrightarrow C_2H_4 + H_2 \quad \Delta H_{1123K} = 143 \text{ kJ/mol}; \; K_{1123K} = 2.35 \qquad \text{(Reaction 2)}$$

These factors lead to a net energy demand of 9.75 GJ per ton of HVP with an estimated exergy loss of 13 GJ/ton HVP. Membrane technology is promising for lowering separation costs (Bernardo and Drioli, 2010; Bessarabov et al., 1995; Lin et al., 2018), but it does not address the appreciable exergy losses and carbon emissions incurred in the cracking process. Several alternative ethylene production technologies have been investigated to tackle the upstream exergy losses (see Figure 1). Oxidative coupling of

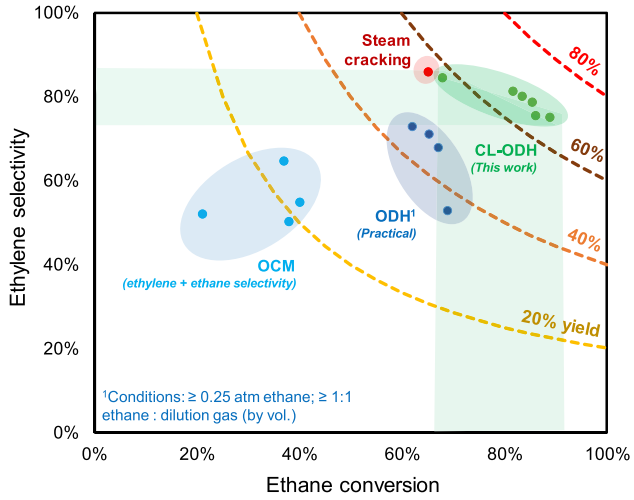

Figure 2. Representative Ethylene Selectivity versus Ethane Conversion Chart

methane (OCM), which converts methane to ethane, ethylene, and water in a set of net-exothermic reactions, has received renewed attention owing to the abundance of inexpensive natural gas produced from North American shale (Arndt et al., 2012; Chua et al., 2008; Jenkins, 2012; Ahari et al., 2011; Elkins and Hagelin-Weaver, 2013, 2015). However, the low single-pass ethylene yields (<20% ethylene) and considerable ethane by-product (Ahari et al., 2011; Elkins and Hagelin-Weaver, 2015, 2013) require intensive downstream separation and recycle of unconverted methane and ethane.

In the ethane ODH route (Reaction 4), ethane is selectively oxidized to ethylene and water, which can potentially reduce reaction exergy losses and downstream separation costs (Henning and Schmidt, 2002; Al-Ghamdi et al., 2013a; 2013b; Argyle et al., 2002; Qiao et al., 2014). The removal of hydrogen as water pushes the system toward higher equilibrium conversions. The water product can be efficiently removed by condensation, lowering downstream separation loads. Single-pass ethylene yields as high as 78.3% (~87% selectivity) have been reported for the Mo, V, Te, Nb mixed oxide "M1" catalysts (Xie et al., 2005). However, the use of gaseous oxygen increases parasitic energy consumption from cryogenic air separation (Castle, 2002; Smith and Klosek, 2001) and raises safety concerns. It is also difficult to maintain a combination of high selectivity and high conversion at the same time, limiting single-pass yields. Although several promising co-feed catalysts have been identified (Henning and Schmidt, 2002; Botella et al., 2004; Cavani et al., 2007; Cavani and Trifirò, 1995; Sanchis et al., 2017; Santander et al., 2014; Xie et al., 2005), few have demonstrated industrially satisfactory single-pass yields (e.g., >50%) at commercially relevant conditions (>1:1 ethane: diluent by volume). Figure 2 maps the performance of these alternative routes with respect to ethane steam cracking.

OCM

$$2{\cdot}CH_4 + O_2 \rightarrow C_2H_4 + 2{\cdot}H_2O \cdots\cdots\cdots \Delta H = -280.3\ \text{kJ/mol} \qquad \text{(Reaction 3)}$$

Ethane ODH

$$C_2H_6 + {}^1\!/_2{\cdot}O_2 \rightarrow C_2H_4 + H_2O \cdots\cdots\cdots \Delta H = -105.5\ \text{kJ/mol} \qquad \text{(Reaction 4)}$$

The CL-ODH process eliminates the challenges of traditional ODH and OCM (Haribal et al., 2017; Neal et al., 2016; Yusuf et al., 2017). The sensible heat in the oxidized redox catalyst particles (Reaction 1b) drives the endothermic gas-phase cracking reactions (Reaction 1a). As illustrated in Figure 3, conventional cracking would result in an inevitable exergy loss of >1.7 GJ per ton of produced ethylene, under an ideal scenario of (1) 100% ethylene yield, (2) perfect heat utilization for cracking, and (3) zero steam dilution. In comparison, even without accounting for its several practical advantages, CL-ODH reduces this minimum exergy loss by 27%. This exergy-saving primarily stems from the *in situ* hydrogen combustion occurring in

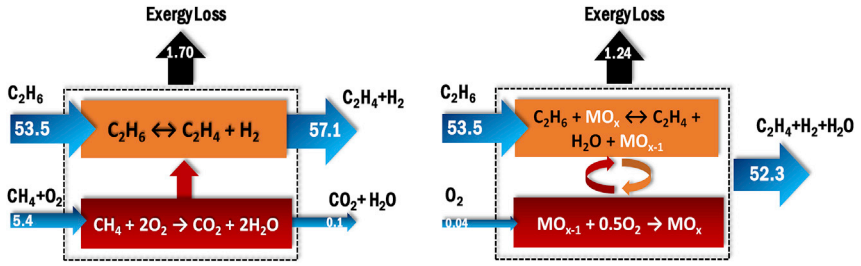

Figure 3. Idealized Exergy Conversion/Loss for Cracking and CL-ODH Schemes at 850°C (GJ/Ton Ethylene)

CL-ODH versus the combustion of externally supplied methane, in conventional cracking. At an industrial scale, these CL-ODH reactions will be carried out in a circulating fluidized bed system with continuous circulation of redox catalyst particles. Compared with conventional ODH, CL-ODH can improve the ethylene yield and process safety while eliminating the costly and energy-intensive cryogenic air separation step.

Redox Catalyst Performance and Demonstration

Our previous work has demonstrated a Mg_6MnO_8-based, model redox catalyst with excellent redox kinetics and single-pass ethylene yields of up to 68% (Neal et al., 2016). In this work a significantly improved, prototype CL-ODH redox catalyst (Sofranko et al., 2016) was demonstrated for improved catalyst selectivity, activity, and physical stability. Structural promotion is essential in ensuring sufficient physical and chemical stability of the catalyst, which is crucial for fluidization in a reactive atmosphere at 850°C without considerable attrition or unacceptable drops in activity. Details with respect to the redox catalyst composition can be found in *Example 1 (Bed D)* in Sofranko et al. (2016). To obtain a preliminary determination of the chemical/redox stability of this new, prototype redox catalyst, it was first tested in a packed-bed U-tube reactor for 115 redox cycles at 1,200 h^{-1} GHSV/1.6 h^{-1}WHSV (Gas Hourly and Weight Hourly Space Velocity) and 850°C (see Supplemental Information 1.1). The prototype demonstrated up to 74% olefin yield with high C_{2+} selectivity, over multiple cycles, as shown in Figure 4 (also see Table S1). The product distribution from CL-ODH is similar to that from thermal cracking (see Figure 4 and Table S6), with key differences in higher yields toward C_{3+} (particularly 1,3-butadiene) and formation of small amounts of CO_2 and CO (~4% total yield on a carbon basis). This can be attributed to the combustion of hydrogen by the redox catalyst, which shifts the equilibrium of gas-phase cracking reactions toward heavier products. Overall, more than 75% of H_2 was converted to water, which is sufficient to meet the energy demand of the overall reaction. The prototype is highly stable over 115 cycles, which is indicative of its long-term stability. Over the course of the reactions, a slight loss of selectivity (89.6% versus 88.2% C_{2+}) is observed but is accompanied by a slight increase in overall conversion (83.1% versus 86.6% conversion). Fluidized-bed testing demonstrates the chemical and physical stability of the prototype for 1,400 cycles during 10 days of continuous operation. As illustrated in Figure 5 (also see Figures S1 and S2), the redox catalyst is highly promising for the proposed CL-ODH process.

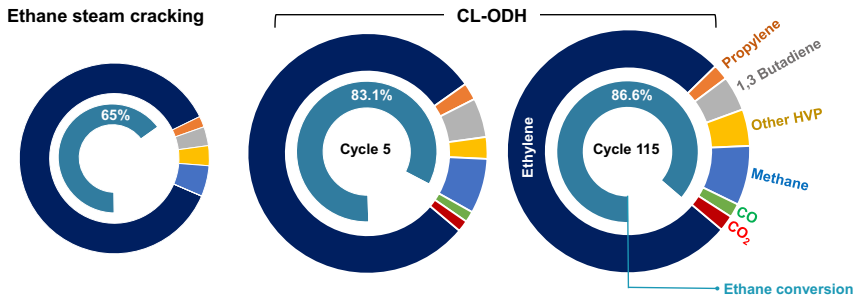

Figure 4. Product Selectivity (Carbon Basis) and Ethane Conversions in Ethane Steam Cracking versus That Obtained Using the Prototype Catalyst after 5 and 115 Cycles in the U-tube Reactor
(See Figure S1 and Table S1).

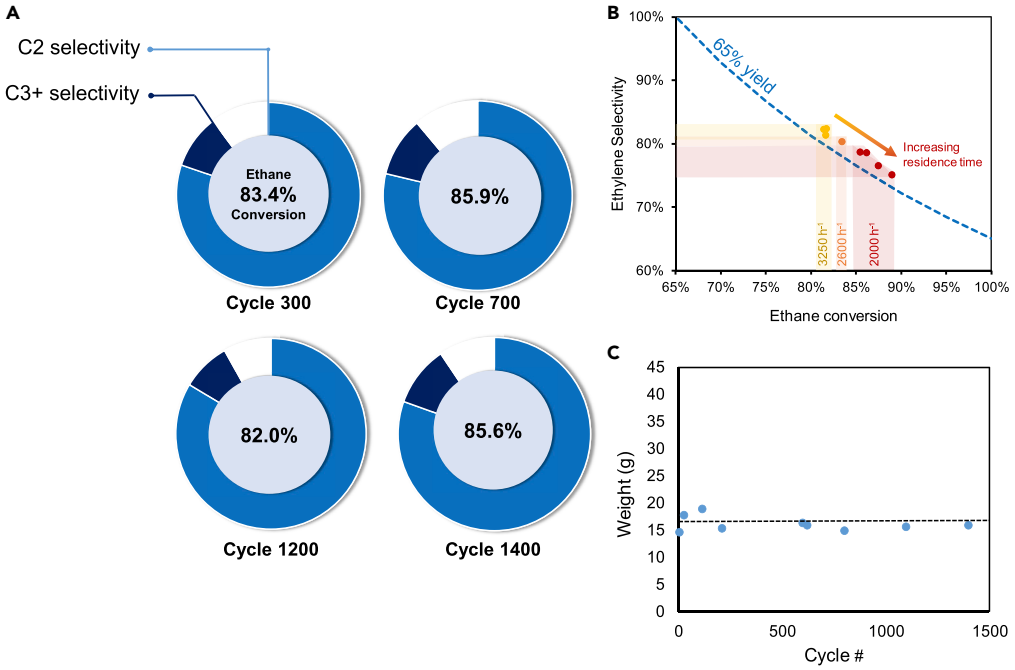

Figure 5. Fluidized-Bed Redox Catalyst Performance

(A) Conversion and selectivity of prototype redox catalyst over 1,400 cycles. (B) Ethylene selectivity versus ethane conversion in a fluidized bed at multiple gas hourly space velocities, over 1,400 cycles (typical conditions: 16 g catalyst, 845°C, 15%–30% ethane, GHSV: 2000 hr^{-1} – 3250 hr^{-1}); (C) 1,400-cycle fluidized bed testing demonstrating superior physical stability of the prototype redox catalyst.

Process Analysis: Steam Cracking versus CL-ODH

Depending on the gas residence time and solids hold-up in the fluidized bed reactor, CL-ODH offers flexibility in terms of ethane conversion and overall process exothermicity, since ethane conversion in CL-ODH is not limited by a reaction equilibrium as is the case with steam cracking. Detailed comparisons of CL-ODH at 85% ethane conversion (ODH 85) and steam cracking are performed through *AspenPlus* process simulations (see Supplemental Information 1.2). Additionally, we have also analyzed two other ethane conversion cases, i.e., ODH 67 (67% conversion based on experimental data) and ODH 99 (to evaluate an idealized scenario via extrapolation of experimental data). Compared with our previous study (Haribal et al., 2017), the current model provides significantly greater detail with respect to heat integration and downstream separations.

Table 1 provides a section-wise comparison of energy consumption (also see Table S7). The simulation indicates energy demands of 21.13 GJ/ton HVP for steam cracking versus 5.09 for ODH 85. This corresponds to a net decrease of 15.7 GJ/ton HVP or 76% in primary energy consumption (see Figure S7). It is noted that both CL-ODH and steam cracking co-produce H_2 and CH_4. For CL-ODH, a notable amount of CO is also produced (see Figure 4, Tables S5 and S6). These compounds can either be credited to the process as fuels or purified and sold as by-products. Accounting for these by-products as fuel (using the Lower Heating Value or LHV) produces a credit of 11.38 and 7.30 GJ/ton HVP for steam cracking and ODH 85, respectively. The fuel credit for ODH 85 is partially offset by an additional ethane demand due to lower C_{2+} selectivity. Accounting for these credits, ODH 85 produces a net reduction in fuel demand of 81%.

Second Law Analysis

Despite the near-perfect thermal efficiencies reported for steam cracking (Tao Ren, 2006; Zimmermann and Walzl, 2000), the source of energy savings achieved by CL-ODH was determined using a detailed second law thermodynamic (i.e., exergy) analysis using AspenPlus (see Supplemental Information 1.3). Exergy analysis is particularly useful in light of the different energy qualities associated with the feedstock, fuels, by-products, and steam. Table 2 compares the section-wise exergy losses in the CL-ODH

		Net Energy Demand/ Recovery (GJ_{Th}/ton HVP)	
		Steam Cracking	ODH 85
Demand	Radiant Zone of the Cracking Furnace	6.63	
	ODH Reactor-Regenerator Pair	NA	−1.3
	Preheating and Heat Recovery	9.55	2.62
	Quench[a]	−3.92	−2.93
	Compression	3.31	2.04
	Refrigeration	2.37	1.31
	Hydrocarbon Separation	3.19	2.85
	CO_2 recovery and Acetylene Removal	0	0.5
	Total Demand	**21.13**	**5.09**
Fuel credits and penalties	Fuel Gas By-product (CO, H_2, and CH_4) (LHV)	−11.38	−7.3
	Extra Ethane Feed	0 (by definition)	4.04
Net demand		**9.75**	**1.83**

Table 1. Section-wise Energy/Fuel Demand of Steam Cracking and ODH 85

(Also see Table S7).

[a]Steam cracking units and the proposed CL-ODH scheme recover a significant amount of heat from reactor furnaces and the product system quench.

cases with steam cracking. With respect to steam cracking, ODH 85 has a net exergy saving of 4.26 GJ/ton HVP with the prime share occurring in the reactors (2.84 GJ/ton HVP). The current simulation indicates little exploitable energy (0.093 GJ/ton HVP) in the exhaust stream for steam cracking, confirming high thermal (first law) efficiency. However, in the cracker, a large destruction of exergy occurs in the

Section			Lost Work (GJ/Ton HVP)			
			Steam Cracking	ODH 67	ODH 85	ODH 99
Upstream	Radiant Zone		4.90			
	ODH Reactor-Regenerator Pair		NA	1.64	2.06	2.03
	Power Generation[a]	Preheating and Heat Recovery	2.73	2.21	2.15	2.11
		Quench	1.54	1.30	1.18	1.06
Downstream		Power Generation Block	1.12	1.44	1.34	1.24
	Compression		0.48	0.34	0.31	0.27
	Refrigeration		0.70	0.45	0.35	0.31
	CO_2 and Acetylene Removal		0.10	0.18	0.22	0.18
	Separation		1.43	1.44	1.13	1.05
Total			13.00	8.99	8.74	8.26
% Reduction				30.8	32.7	36.5

Table 2. Section-wise Exergy Loss Analysis

(Also see Table S10).

[a]The Heat Recovery and Quench sections produce steam utilized for power generation.

radiant/cracking and convective zones combined, amounting to 7.6 GJ/ton HVP. As such, even at the reported efficiencies of up to 95% (Zimmermann and Walzl, 2000) (which requires partial condensation in the flue gas stream), sizable exergy losses are inevitable in conventional cracking owing to the irreversibility of fuel combustion and indirect heat transfer, as well as the low quality of the heat recovered.

The idealized analysis in Figure 3 indicates potential exergy savings using hydrogen instead of methane as the fuel. Although substitution of fuels cannot be made without changing other process conditions, a direct comparison of the exergy versus lower heating values of H_2 and methane indicates that the use of hydrogen as fuel is responsible for 1.4 GJ/ton HVP in apparent exergy savings. The remaining 2.1–2.4 GJ difference between the CL-ODH and steam cracking cases, in the reactor/preheating sections, is attributed to the significantly improved heat integration and elimination of steam dilution. Of particular note for steam cracking is the 350°C temperature differential between the radiant zone of the fire box and the highest temperature inside the cracking coils. This corresponds to a major irreversibility. In contrast, CL-ODH directly utilizes the sensible heat in the oxygen carrier particles to supply the heat required for ethane cracking, thereby minimizing the irreversibility.

The exergy savings of CL-ODH in the downstream of the process, illustrated in Figure 6 and Table 2 (also see Figure S7), is relatively straightforward. The removal of hydrogen as condensed water in CL-ODH prominently reduces the volume of gas that must be compressed and refrigerated (37% volume reduction). Combined with a higher per-pass yield, the quench, compression, and refrigeration sections in CL-ODH can result in up to a 0.9 GJ/ton HVP reduction in exergy loss. In spite of the higher overall downstream power demand, the exergy loss in the power generation section of steam cracking appears to be less than that of the CL-ODH cases. This results from the need to burn more fuel directly for power generation due to less heat recovery from the CL-ODH reactors. However, the improved power generation in steam cracking does not offset the large exergy losses in the furnace. When exergy losses in the pre-heating/heat recovery and quench are included in power generation, CL-ODH reduces exergy loss by 0.44–0.97 GJ/ton HVP (see Table 2) in these sections.

Exergy savings for CL-ODH in the separation sections are more limited than in the upstream section (see Table S10). This is attributed to a combination of (1) the need for CO removal before acetylene hydrogenation and (2) the inherently heavy separation demands imposed by polymer-grade ethylene specifications. The CL-ODH reaction product contains sufficiently high CO to poison the catalyst used for acetylene removal via selective hydrogenation (Battiston et al., 1982; Schbib et al., 1996). This necessitates the placement of acetylene removal (the de-acetylenizer) after the de-ethanizer, requiring an additional heat exchange load. Polymer-grade ethylene purity requirements (99.99%) impose a high exergy loss in the C2 splitter. This is the case even for the ODH 99 case with 99% ethane conversion (0.487 GJ/ton HVP). This underscores the potential impact of membranes and other advanced hydrocarbon separation technologies on ethylene production.

Broader Impact on CO_2 Emission Reduction

CL-ODH's higher exergetic efficiency also leads to substantial reduction in CO_2 emissions. A comparison of CO_2 emissions is given in Table 3 and Figure 7 (also see Figure S9). If fuel gas by-products are exported without credit, steam cracking gives CO_2 emissions of 1.26 ton/ton HVP, consistent with other simulations in the literature (Tao Ren, 2006). By comparison, ODH 85 emits only 0.45 ton/ton HVP, leading to a 64% reduction, as shown in Table 3. If the hydrogen is separated and recovered (at the cost of additional energy for pressure swing adsorption), it may be credited as a zero-carbon fuel against methane. Additionally, the CL-ODH cases also capture CO_2 in the product separation section, which, if beneficially utilized or sequestered, reduces the CO_2 emissions of the process. When hydrogen is credited as a by-product (at LHV) and the 0.093 ton of captured CO_2/ton HVP in the CL-ODH cases are credited, the ODH 85 emits 0.19 ton of CO_2/ton HVP. This represents a 78% reduction compared with steam cracking (0.88 ton CO_2/ton HVP). On a commercial scale of 1.5 million tons per annum (MTA) plant, this corresponds to a reduction of over 1 million tons of CO_2 each year.

Multiple justifiable assumptions can be made about the crediting of hydrogen as either a low-carbon fuel or an industrial feedstock. For example, although hydrogen can be utilized as a low-carbon fuel in conventional cracking, burning fuel-gas with high hydrogen concentrations can lead to high NO_x emissions (İlbas et al., 2005), requiring costlier emissions control. Additionally, in highly integrated areas, hydrogen can be a

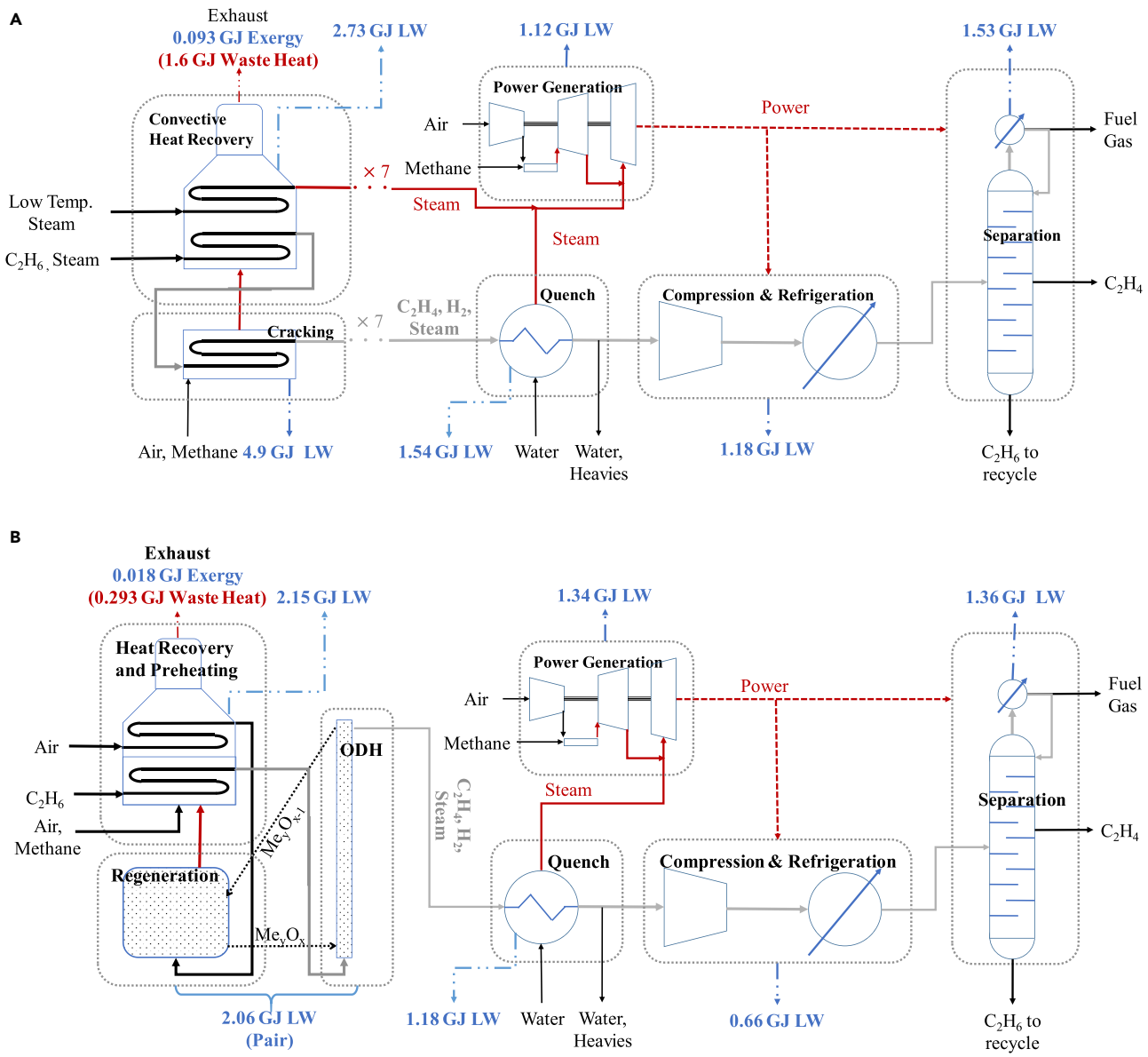

Figure 6. Process and Exergy/Lost Work (LW) Schematics

(A) Steam cracking of ethane and (B) CL-ODH of Ethane (Results are in GJ/ton of high value products).

valuable feedstock for processes such as the production of low-sulfur fuel via hydrodesulfurization (Grange, 1980; Pecoraro and Chianelli, 1981). In this case of integrated chemical use, crediting hydrogen at a rate consistent with displacing steam methane reforming is reasonable (using 9 kg CO_2/kg H_2 [Spath and Mann, 2000]). However, although the various values of the hydrogen by-product credit can affect the absolute value of the overall net CO_2 emissions, it does not change the overall trend between cases. For lower credits, the purification and transportation challenges for hydrogen can make it less carbon intensive to burn the hydrogen as a fuel rather than export it. The trend in CO_2 emissions is consistent with the energy demand and exergy loss trends (CO_2 from Steam Cracking >> ODH 67 > ODH 85 > ODH 99), with the ODH 85 case giving a 60%–87% emission reduction and the ODH 99 case giving a 65%–94% reduction, depending on the assumptions used (see Figure 7). This confirms that the CO_2 reduction of CL-ODH is not an artifact of "fuel substitution" (H_2 versus CH_4). The ability to burn hydrogen without NO_x, while still providing some usable H_2, represents another advantage of CL-ODH.

		Steam Cracking	ODH 85
CO_2 Source	Fuel By-products Burned[a]	0.17	0.32
	External Fuel Burned	1.09	0.035
	CO_2 from Reactor	NA	0.093
	CO_2 Produced	**1.26**	**0.45**
Credits	H_2 Recovery Penalty	0.094	0.027
	Hydrogen Credit (LHV)[b]	−0.47	−0.14
	CO_2 Capture Credit	NA	−0.093
Net CO_2 Emitted		**0.88**	**0.19**

Table 3. CO_2 Production by Source (Ton/Ton HVP)

[a]CO and methane, excludes hydrogen, to eliminate fuel effects on heat recovery fuel gasses are treated as a credit against methane.

[b]Calculated as CO_2 from methane versus the same LHV of hydrogen.

Conclusion

In spite of decades of process optimization and high thermal (first law) efficiency, steam cracking remains an energy- and carbon-intensive process. This is due to large exergy losses incurred by fuel combustion, extensive heat transfer and quench requirements in the cracking furnace, as well as significant compression, refrigeration, and separation loads. Although conventional wisdom dictates the infeasibility of substantial efficiency improvement of steam cracking (which is already 95% thermally efficient), we show that ethylene production can be significantly intensified via exergy loss minimization. The transformative CL-ODH approach has the potential to produce ethylene with near-order of magnitude reduction in energy consumption and CO_2 emissions. The redox catalyst holds the key for the CL-ODH scheme. In this work, we demonstrate the technical feasibility of producing stable, fluidizable, active, and selective redox catalyst particles. Using a prototype redox catalyst, we demonstrate that >85% ethane conversion is achievable while maintaining high selectivity over 1,400 fluidized-bed redox cycles. Modeling of CL-ODH, based on

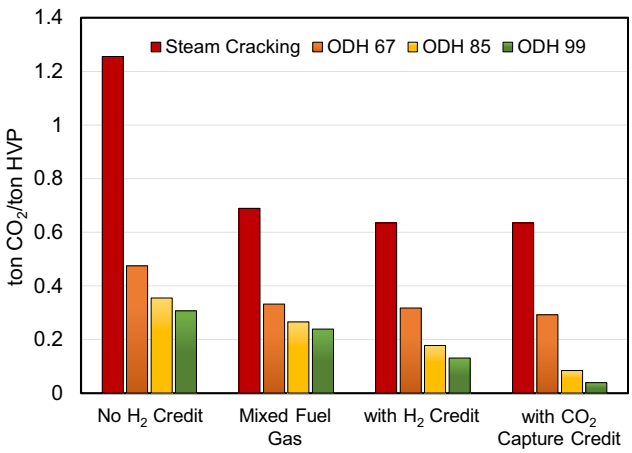

Figure 7. CO_2 Emissions of Steam Cracking and ODH Processes under Various Assumptions:

(1) No H_2 Credit: H_2 is recovered and exported but not credited.

(2) Mixed Fuel Gas: H_2 is not recovered and is burned along with CO and CH_4 as fuel.

(3) with H_2 credit: H_2 is recovered and credited at 9 kg CO_2/kg H_2 (Spath and Mann, 2000).

(4) CO_2 Capture Credit: H_2 is recovered and credited at 9 kg CO_2/kg H_2 and CO_2 recovered from ODH product stream is beneficially utilized and not emitted.

Fuel gas and mixed fuel gas are calculated as a credit against methane burned to eliminate fuel composition effects on flue gas heat recovery. The Mixed Fuel Gas, ODH 99 case exports unused fuel gas at no credit.

experimental yields, demonstrates lower exergy loss (second law) per unit of HVP, compared with steam cracking. CL-ODH leads to substantial energy savings in the reactor sections. It also facilitates easier downstream processing owing to removal of hydrogen as condensable water and significant increase in ethane per-pass conversions compared with those attained in steam cracking. This improved efficiency leads to a CO_2 reduction of up to 87%. These findings not only support the feasibility of CL-ODH but also provide a useful guidance to design intensified chemical production processes with significantly lowered emissions. If adopted at a global level, this innovative process can reduce annual CO_2 emissions by over 100 million tons for ethylene production.

Limitations of the Study

The use of RStoic reactor models, along with other simplifying assumptions, may not fully capture complex behavior in a circulating fluidized bed reactor that could be revealed in future pilot scale testing.

METHODS

All methods can be found in the accompanying Transparent Methods supplemental file.

SUPPLEMENTAL INFORMATION

Supplemental Information can be found online at https://doi.org/10.1016/j.isci.2019.08.039.

ACKNOWLEDGMENTS

This work was supported by the U.S. National Science Foundation (Award No. CBET-1604605), the U.S. Department of Energy (RAPID Sub-award DE-EE0007888-05-6), and the Kenan Institute for Engineering, Technology and Science at NC State University. The authors acknowledge the use of the Analytical Instrumentation Facility (AIF) at North Carolina State University, which is supported by the State of North Carolina and the National Science Foundation.

AUTHOR CONTRIBUTIONS

F.L. conceived and supervised the work. L.M.N. and F.L. designed the study. L.M.N., V.P.H., and F.L. wrote the manuscript. V.P.H. carried out process simulations and exergy analyses. L.M.N. synthesized the redox catalyst, carried out the experiments, and analyzed the data.

DECLARATION OF INTERESTS

L.M.N. and F.L. are co-inventors and retain financial interests in patents covering the prototype redox catalysts for CL-ODH and other CL-ODH systems.

Received: June 2, 2019
Revised: August 6, 2019
Accepted: August 21, 2019
Published: September 27, 2019

REFERENCES

Ahari, J.S., Sadeghi, M.T., and Zarrinpashne, S. (2011). Effects of operating parameters on oxidative coupling of methane over Na-W-Mn/SiO_2 catalyst at elevated pressures. J. Nat. Gas Chem. *20*, 204–213.

Al-Ghamdi, S.A., Hossain, M.M., and de Lasa, H.I. (2013a). Kinetic modeling of ethane oxidative dehydrogenation over VOx/Al_2O_3 catalyst in a fluidized-bed riser simulator. Ind. Eng. Chem. Res. *52*, 5235–5244.

Al-Ghamdi, S., Volpe, M., Hossain, M.M., and de Lasa, H. (2013b). VOx/c-Al_2O_3 catalyst for oxidative dehydrogenation of ethane to ethylene: desorption kinetics and catalytic activity. Appl. Catal. Gen. *450*, 120–130.

Andrews, A.J., and Pollock, L.W. (1959). Tube by tube design of light hydrocarbon cracking furnaces using a digital computer. Ind. Eng. Chem. *51*, 125–128.

Argyle, M.D., Chen, K., Bell, A.T., and Iglesia, E. (2002). Ethane oxidative dehydrogenation pathways on vanadium oxide catalysts. J. Phys. Chem. B *106*, 5421–5427.

Arndt, S., Otremba, T., Simon, U., Yildiz, M., Schubert, H., and Schomäcker, R. (2012). Mn–Na_2WO_4/SiO_2 as catalyst for the oxidative coupling of methane. What is really known? Appl. Catal. Gen. *425–426*, 53–61.

Battiston, G.C., Dalloro, L., and Tauszik, G.R. (1982). Performance and aging of catalysts for the selective hydrogenation of acetylene: a micropilot-plant study. Appl. Catal. *2*, 1–17.

Bernardo, P., and Drioli, E. (2010). Membrane gas separation progresses for process intensification strategy in the petrochemical industry. Pet. Chem. *50*, 271–282.

Bessarabov, D.G., Sanderson, R.D., Jacobs, E.P., and Beckman, I.N. (1995). High-efficiency separation of an ethylene/ethane mixture by a large-scale liquid-membrane contactor containing flat-sheet nonporous polymeric gas-separation membranes and a selective flowing-liquid absorbent. Ind. Eng. Chem. Res. *34*, 1769–1778.

Boot-Handford, M.E., Abanades, J.C., Anthony, E.J., Blunt, M.J., Brandani, S., Mac Dowell, N., Fernández, J.R., Ferrari, M.C., Gross, R., Hallett, J.P., et al. (2014). Carbon capture and storage update. Energy Environ. Sci. *7*, 130–189.

Botella, P., García-González, E., Dejoz, A., López Nieto, J.M., Vázquez, M.I., and González-Calbet, J. (2004). Selective oxidative dehydrogenation of ethane on MoVTeNbO mixed metal oxide catalysts. J. Catal. *225*, 428–438.

Brown, D.E., Clark, J.T.K., Foster, A.I., McCarroll, J.J., and Sims, M.L. (1983). Inhibition of coke formation in ethylene steam cracking. In Coke Formation on Metal Surfaces, L.F. Albright and R.T.K. Baker, eds. (American Chemical Society), pp. 23–43.

Castle, W.F. (2002). Air separation and liquefaction: recent developments and prospects for the beginning of the new millennium. Int. J. Refrig *25*, 158–172.

Cavani, F., and Trifirò, F. (1995). The oxidative dehydrogenation of ethane and propane as an alternative way for the production of light olefins. Catal. Today *24*, 307–313.

Cavani, F., Ballarini, N., and Cericola, A. (2007). Oxidative dehydrogenation of ethane and propane: how far from commercial implementation? Catal. Today *127*, 113–131.

Chua, Y.T., Mohamed, A.R., and Bhatia, S. (2008). Oxidative coupling of methane for the production of ethylene over sodium-tungsten-manganese-supported-silica catalyst (Na-W-Mn/SiO_2). Appl. Catal. Gen. *343*, 142–148.

Elkins, T.W., and Hagelin-Weaver, H.E. (2013). Oxidative coupling of methane over unsupported and alumina-supported samaria catalysts. Appl. Catal. Gen. *454*, 100–114.

Elkins, T.W., and Hagelin-Weaver, H.E. (2015). Characterization of Mn–Na_2WO_4/SiO_2 and Mn–Na_2WO_4/MgO catalysts for the oxidative coupling of methane. Appl. Catal. Gen. *497*, 96–106.

Ethylene Global Supply Demand Analytics Service (2018). Verisk Analytics. https://www.woodmac.com/news/editorial/ethylene-global-supply-demand-analytics-service/.

Figueroa, J.D., Fout, T., Plasynski, S., McIlvried, H., and Srivastava, R.D. (2008). Advances in CO_2 capture technology—the U.S. Department of energy's carbon sequestration program. Int. J. Greenh. Gas Control *2*, 9–20.

Friedrich, J. (2019). Greenhouse gas emissions over 165 years. World Resour. Inst.. https://www.wri.org/resources/data-visualizations/greenhouse-gas-emissions-over-165-years

Global Emissions (2017). Cent. Clim. Energy Solut.. https://www.c2es.org/content/international-emissions/

Grange, P. (1980). Catalytic hydrodesulfurization. Catal. Rev. *21*, 135–181.

Griffin, D.E., Moon, J.J.. (1964). Separation of gases. US3119677 A.

Haribal, V.P., Neal, L.M., and Li, F. (2017). Oxidative dehydrogenation of ethane under a cyclic redox scheme – process simulations and analysis. Energy *119*, 1024–1035.

Henning, A., and Schmidt, D. (2002). Oxidative dehydrogenation of ethane at short contact times: species and temperature profiles within and after the catalyst. Chem. Eng. Sci. *57*, 2615–2625.

Heynderickx, G.J., Oprins, A.J.M., Marin, G.B., and Dick, E. (2001). Three-dimensional flow patterns in cracking furnaces with long-flame burners. AIChE J. *47*, 388–400.

İlbas, M., Yılmaz, İ., and Kaplan, Y. (2005). Investigations of hydrogen and hydrogen–hydrocarbon composite fuel combustion and NOx emission characteristics in a model combustor. Int. J. Hydrog. Energy *30*, 1139–1147.

Jenkins, S. (2012). Shale gas ushers in ethylene feed shifts. Chem. Eng. N. Y. *119*, 17–19.

Li, F., Neal, L.M.. (2017). Ethylene Yield in Oxidative Dehydrogenation of Ethane and Ethane Containing Hydrocarbon Mixtures. 20170226030.

Li, B., Duan, Y., Luebke, D., and Morreale, B. (2013). Advances in CO_2 capture technology: a patent review, In Special Issue on Advances in sustainable biofuel production and use - XIX International Symposium on Alcohol Fuels - ISAF. Appl. Energy *102*, 1439–1447.

Lin, R.-B., Li, L., Zhou, H.-L., Wu, H., He, C., Li, S., Krishna, R., Li, J., Zhou, W., and Chen, B. (2018). Molecular sieving of ethylene from ethane using a rigid metal–organic framework. Nat. Mater. *17*, 1128–1133.

Ludwig, K.. (1951). Production of ethylene. US2573341 A.

Masaaki, K., Masaaki, T.. (1967). Process for the separation and purification of ethylene. US3324194 A.

Neal, L.M., Yusuf, S., Sofranko, J.A., and Li, F. (2016). Oxidative dehydrogenation of ethane: a chemical looping approach. Energy Technol. *4*, 1200–1208.

Pecoraro, T.A., and Chianelli, R.R. (1981). Hydrodesulfurization catalysis by transition metal sulfides. J. Catal. *67*, 430–445.

Plehiers, P.M., Reyniers, G.C., and Froment, G.F. (1990). Simulation of the run length of an ethane cracking furnace. Ind. Eng. Chem. Res. *29*, 636–641.

Qiao, A., Kalevaru, V.N., Radnik, J., Düvel, A., Heitjans, P., Kumar, A.S.H., Prasad, P.S.S., Lingaiah, N., and Martin, A. (2014). Oxidative dehydrogenation of ethane to ethylene over V_2O_5/Al_2O_3 catalysts: effect of source of alumina on the catalytic performance. Ind. Eng. Chem. Res. *53*, 18711–18721.

Ranjan, P., Kannan, P., Al Shoaibi, A., and Srinivasakannan, C. (2012). Modeling of ethane thermal cracking kinetics in a pyrocracker. Chem. Eng. Technol. *35*, 1093–1097.

Ruckaert, M.J., Martens, X.M., and Desarnauts, J. (1978). Ethylene plant optimization by geometric programming. Comput. Chem. Eng. *2*, 93–97.

Sanchis, R., Delgado, D., Agouram, S., Soriano, M.D., Vázquez, M.I., Rodríguez-Castellón, E., Solsona, B., and Nieto, J.M.L. (2017). NiO diluted in high surface area TiO_2 as an efficient catalyst for the oxidative dehydrogenation of ethane. Appl. Catal. Gen. *536*, 18–26.

Santander, J., López, E., Diez, A., Dennehy, M., Pedernera, M., and Tonetto, G. (2014). Ni–Nb mixed oxides: one-pot synthesis and catalytic activity for oxidative dehydrogenation of ethane. Chem. Eng. J. *255*, 185–194.

Sato, T., and Ohnishi, Y. (1971). A new quench boiler for the ethylene plant. Bull. Jpn. Pet. Inst. *13*, 279–284.

Schbib, N.S., García, M.A., Gígola, C.E., and Errazu, A.F. (1996). Kinetics of front-end acetylene hydrogenation in ethylene production. Ind. Eng. Chem. Res. *35*, 1496–1505.

Smith, A.R., and Klosek, J. (2001). A review of air separation technologies and their integration with energy conversion processes. Fuel Process. Technol. *70*, 115–134.

Socolow, R.H., and Pacala, S.W. (2006). A plan to keep carbon in check. Sci. Am. *295*, 50–57.

Sofranko, J.A., Li, F., Neal, L.. (2016). Oxygen transfer agents for the oxidative dehydrogenation of hydrocarbons and systems and processes using the same. WO2016049144A1.

Spath, P.L., and Mann, M.K. (2000). Life Cycle Assessment of Hydrogen Production via Natural Gas Steam Reforming (No. NREL/TP-570-27637) (National Renewable Energy Lab.).

Tao Ren, M.P. (2006). Olefins from conventional and heavy feedstocks: energy use in steam cracking and alternative processes. Energy *31*, 425–451.

Tola, V., and Pettinau, A. (2014). Power generation plants with carbon capture and storage: a techno-economic comparison between coal combustion and gasification technologies. Appl. Energy *113*, 1461–1474.

Volkart, K., Bauer, C., and Boulet, C. (2013). Life cycle assessment of carbon capture and storage in power generation and industry in Europe. Int. J. Greenh. Gas Control *16*, 91–106.

W, P.L. (1963). Furnace control. US3112880 A.

Xie, Q., Chen, L., Weng, W., and Wan, H. (2005). Preparation of MoVTe(Sb)Nb mixed oxide catalysts using a slurry method for selective oxidative dehydrogenation of ethane. J. Mol. Catal. Chem. *240*, 191–196.

Yusuf, S., Neal, L.M., and Li, F. (2017). Effect of promoters on manganese-containing mixed metal oxides for oxidative dehydrogenation of ethane via a cyclic redox scheme. ACS Catal. *7*, 5163–5173.

Zimmermann, H., and Walzl, R. (2000). Ethylene, in: Ullmann's Encyclopedia of Industrial Chemistry (Wiley-VCH Verlag GmbH & Co. KGaA).

ISCI, Volume *19*

Supplemental Information

Intensified Ethylene Production via Chemical Looping through an Exergetically Efficient Redox Scheme

Luke M. Neal, Vasudev Pralhad Haribal, and Fanxing Li

Figures

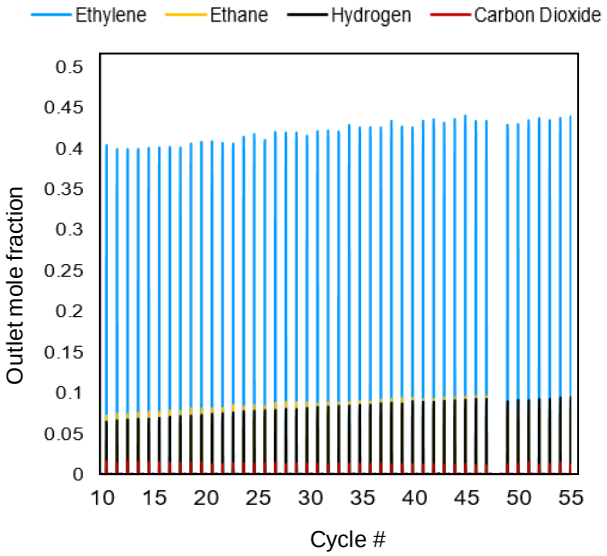

Figure S1*: QMS Trace of Cycles 10-55 in the U-tube. Gap at cycle 48 represents gas-bag samples as reported in Table S1* (Related to Figure 4)

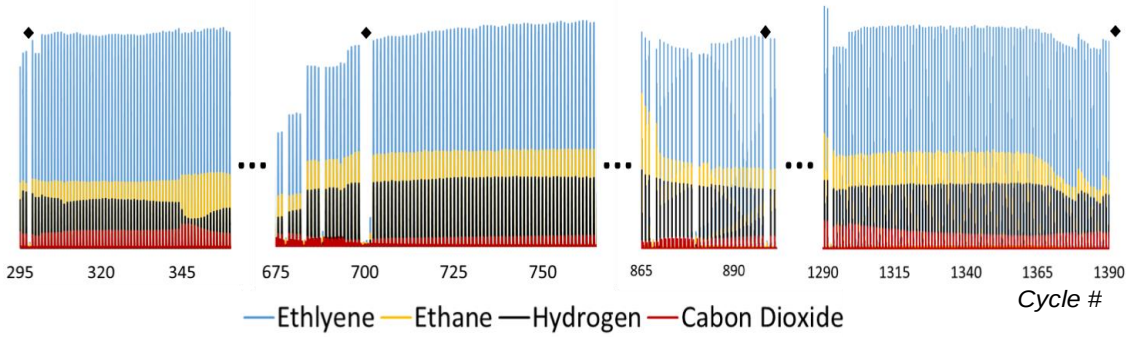

Figure S2: *Compiled QMS signal from the 1400 cycle testing. Diamonds corresponds to the cycles shown in Table S2 where a gas bag and gas chromatography was used to analyze detailed product compositions. Variation in QMS signal was reduced from varying operating conditions during the continuous testing such as space velocity, ethane concentration, and O_2 concentration (also see 1.1 above for the conditions)* (Related to Figure 5)

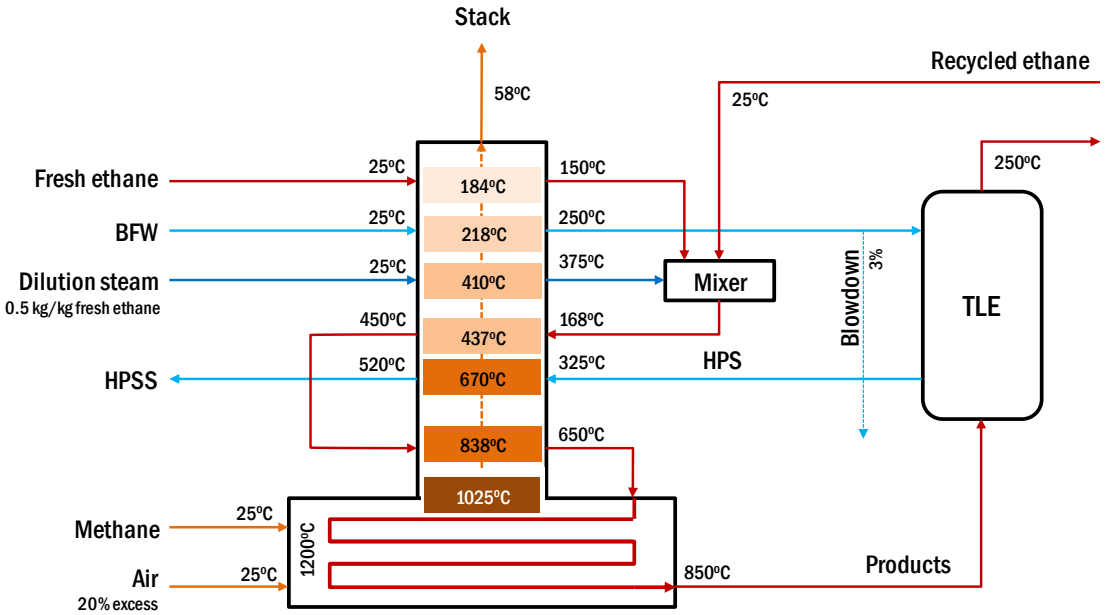

***Figure S3**: Modeling the ethane steam cracking process (Sadrameli, 2015)* (Related to Figure 6 and Table 1)

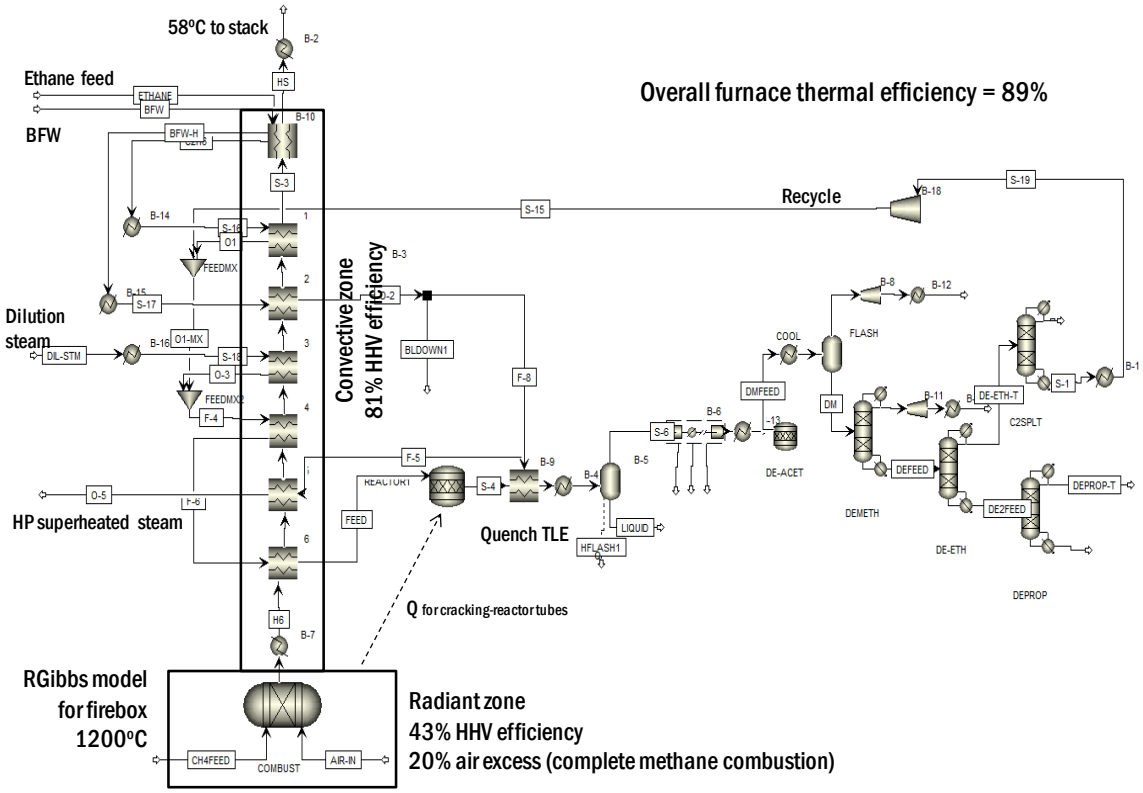

***Figure S4**: AspenPlus® flowsheet for steam cracking (Haribal et al., 2017; Sadrameli, 2015; Zimmermann and Walzl, 2000)*
(Related to Figure 6 and Table 1)

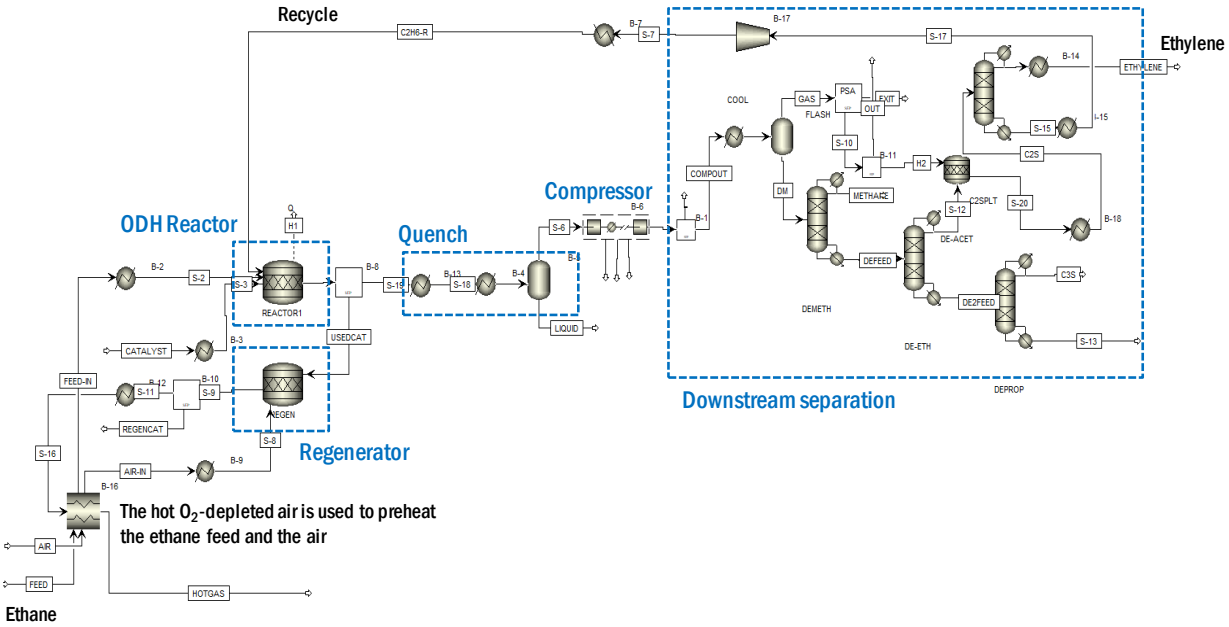

***Figure S5**: AspenPlus® flowsheet for the ODH cases* (Related to Figure 6 and Table 1)

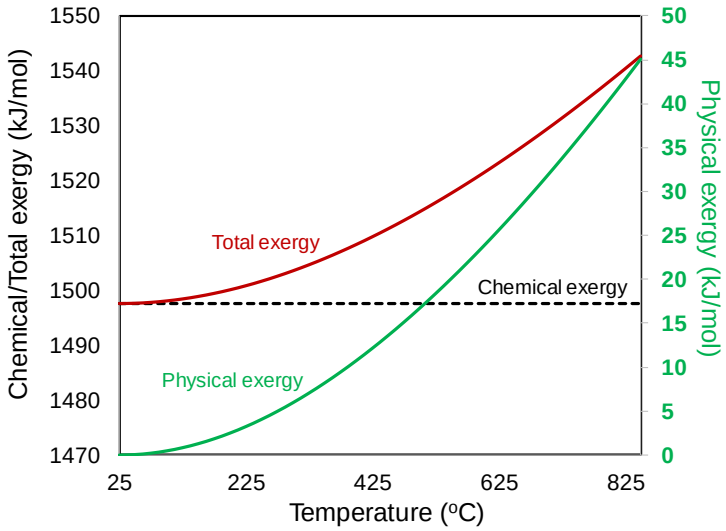

***Figure S6**: Exergy of an ethane stream with change in temperature* (Related to Section 2.4 and Table 2)

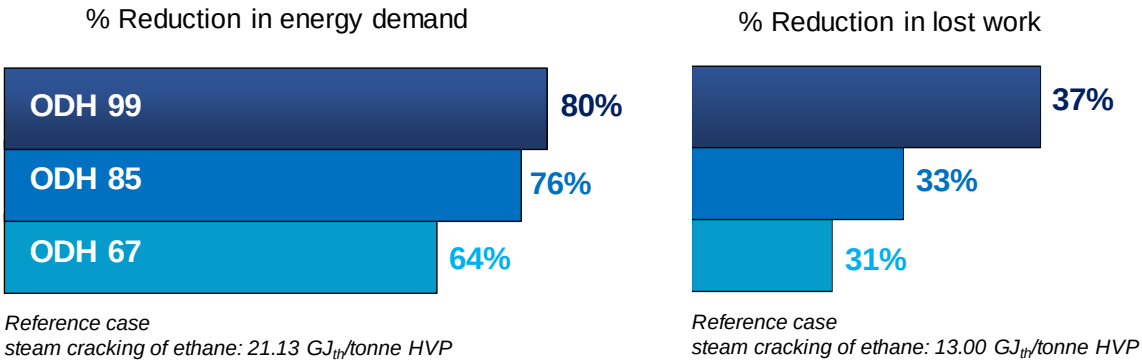

***Figure S7**: Comparison of ODH cases with ethane steam cracking; a) energy demand (left); and b) lost work (right)* (Related to Table 1 and 2)

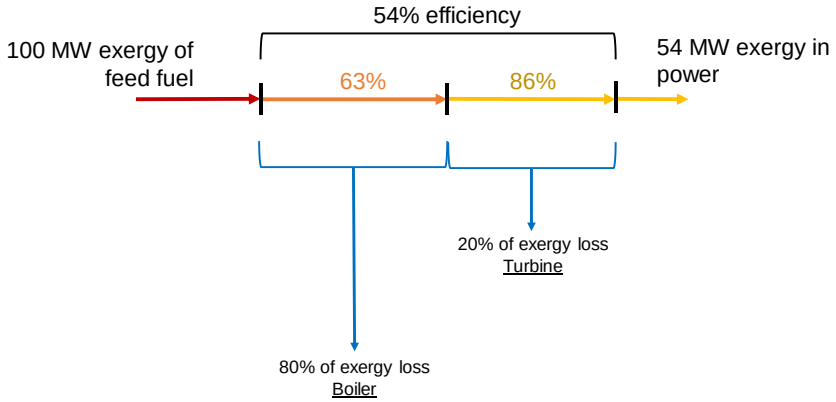

***Figure S8**: Approach for power generation exergy loss* (Related to Figure 6)

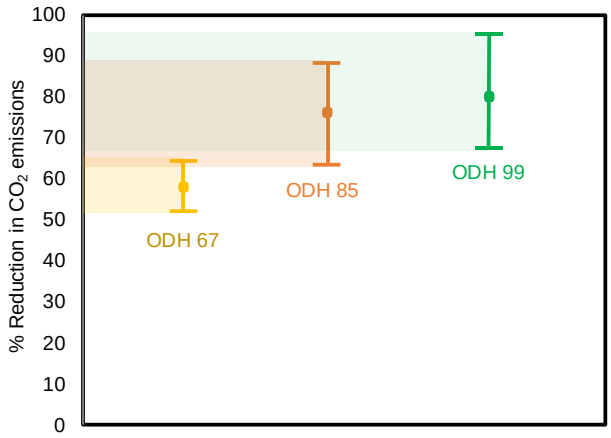

***Figure S9**: % Reduction in CO_2 emissions for the CL-ODH cases in comparison with steam cracking using different assumptions (range of reductions)* (Related to Figure 7 and Table 3)

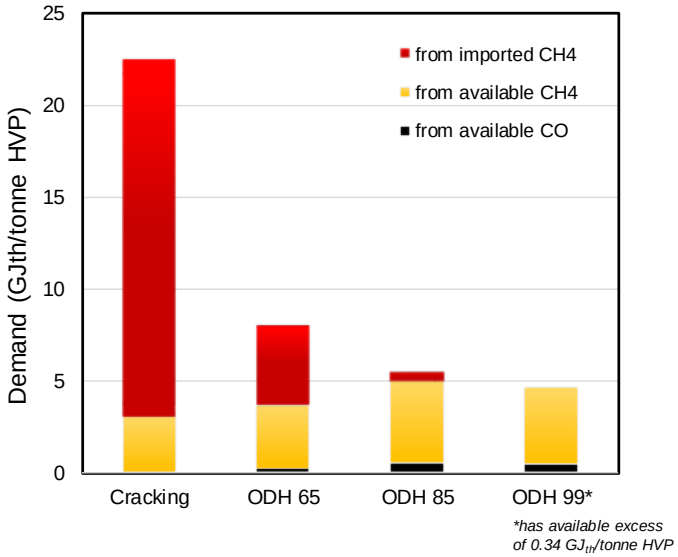

***Figure S10**: Comparison of the available and imported fuel among all the considered cases* (Related to Table 1 and 3)

Transparent Methods

CL-ODH redox catalyst preparation and performance study

The prototype fluidized bed sample is prepared by mixing solutions of alkali hydroxides, tungstate salts and structural promoters into an aqueous slurry of MgO and MnO_2 powder in ratios consistent with the compositions described in *Example 1 (Bed D)* in the patent (*Sofranko et al., 2016*). The resulting slurry is ball-milled, dried, calcined above 900 °C and then sieved. In the **115-cycle U-tube testing**, 2 g of redox catalyst is placed into a 6.3mm O.D. by 4mm I.D. U-tube. α-alumina grit is packed on both sides of the catalyst bed to lower the void volume of the reactor in the heated zone. This gives a total CL-ODH reactor bed volume of approximately 1.25 ml.

The U-tube is placed in an 850 °C tube furnace under a purge of argon. During redox cycling, 10 ml of ethane (80% ethane in argon) is contacted with the catalyst at space velocities of 1200-3000 h^{-1}. After ethane ODH, the tube is purged for 5 min with Ar (5.0 grade), and re-oxidized in 10% O_2 followed by another 5 min of Ar purge before initiating a subsequent redox cycle. A quadrupole mass spectrometer (QMS, MKS Cirrus II) is used to monitor the reaction over several cycles. During select cycles, the ethane ODH product is collected in a gas bag and analyzed using gas chromatography (GC). The GC (Agilent 7890B, refinery gas analyzer configuration) is equipped with an Ar TCD channel for hydrogen analysis, a He TCD for CO and CO_2 analysis, and an FID channel for hydrocarbon quantification. The GC is calibrated with a refinery gas calibration standard (Agilent 5190-0519). The QMS was calibrated with hydrogen, ethane, and ethylene standards, and refined using GC results. Hydrocarbon conversion and yields are calculated using carbon mass balance, with the H_2O-yield calculated by balancing the mass with recovered hydrogen and hydrocarbons. Integration of the water signal from mass spectra is used to confirm the water-balance. Catalyst stability is shown by aging the catalyst for more than 100 cycles (*Figure S1 and Table S1*).

***Table S1**: U-tube fixed bed performance (as depicted in Figure 4) @ 1200 h^{-1} 850 ºC* (Related to Figure 4)

Selectivity	Cycle 5	Cycle 48	Cycle 115
Ethylene	79.1%	76.1%	76.6%
Propylene	2.3%	2.3%	2.2%
1,3 Butadiene	5.3%	5.2%	5.1%
Other HVP	2.9%	5.3%	4.3%
Methane	7.4%	7.3%	7.9%
CO	1.5%	1.8%	1.8%
CO_2	1.5%	2.0%	2.1%
Ethane conversion	**83.1%**	**85.77%**	**86.6%**

In the **1400-cycle fluidized bed tests**, 16 grams (or ~10 ml) of prototype catalyst particles are placed in a 1' O.D. × 0.75' I.D. alumina tube that is mounted in a vertical tube furnace. The fluidized bed is supported in the heated zone by inert 16 mesh SiC grit. Nitrogen is used as the main fluidization gas, with ethane and O_2 being cycled through the system by an automated manifold. Ethane concentration is varied between 15-30 vol. % and O_2 concentrations were varied from 5 to 10%. 80-120 ml of ethane is injected in the reduction step. Variations in operating conditions were made during the 1400 cycle test to obtain a comprehensive understanding of the redox catalyst performance. *Figure 5a (in the main text)* summarizes performance data among cycles operated under identical conditions. After an initial 48 hr/ 240 cycle break-in run to obtain stable redox performance, the catalyst is recovered and sieved back to original size (38-180 μm). ~1 gram

of fresh redox catalyst is added to make up catalyst lost in sieving. 1160 continuous redox cycles are subsequently conducted. *Figure S2 (and Table S2)* illustrates the quadruple mass spectrometer (QMS) signal from the 1400 cycle testing.

***Table S2**: Material performance in a fluidized bed reactor performance for 1400 redox cycles (as depicted in Figure 5)* (Related to Figure 5)

Cycle #	Conversion	C2 selec	C3+ selec
300	83.4	80.2	9.5
700	85.9	78.7	10.2
1200	82.0	83.6	8.3
1400	85.6	80.5	10.1

Simulation methods

A refined process simulation model, building upon our previous work (*Haribal et al., 2017*), is constructed to determine the relative exergy losses and emissions of steam cracking and CL-ODH using AspenPlus®. A sequential modular strategy is employed for the simulations, which also includes solids. The steam cracking furnace is modeled using two zones, namely radiant and convective, as a series of stacked heat exchangers, as shown in *Figure S3* (*Haribal et al., 2017; Sadrameli, 2015*). It shows the upstream section of steam cracking which involves the furnace, dilution steam, feed pre-heating and steam-generation from the quench system using Transverse Line Exchangers (TLE). Major sections of the furnace and the corresponding streams are labeled. The downstream consists of the quench system, the compressor, the refrigeration unit (cold box), pressure-swing adsorption (PSA) unit and the separation columns, as shown in *Figure S4.* The separation scheme is similar to the one described in our previous work (*Haribal et al., 2017*).

For the CL-ODH cases, the furnace is replaced by the two-reactor redox scheme, as shown in *Figure S5*. An RStoic model is used to model the CL-ODH reactors (assumptions in *Tables S3-S4*) which utilizes the experimental product distribution, as listed in *Tables S5 and S6*. The endothermic ODH reactor is assumed to be at 850^{o}C, which is the experimental temperature. For an auto-thermal operation, a ΔT of 100^{o}C is set between the two reactors, with the exothermic regenerator at 950^{o}C. The heat from the regenerator is carried by the oxidized redox catalyst and is utilized in the ODH reactor. 950^{o}C represents an estimated practical upper limitation on the stability of the redox catalyst. The feeds to each of the reactors are preheated to 650^{o}C. For CL-ODH, the 950°C depleted air stream from the regenerator is used to preheat the reactor feeds. As this is insufficient for the complete reactant preheating load, a small furnace is used to supplement preheating (*Figure 6 of main text*). For both CL-ODH and steam cracking, product stream is rapidly quenched. This is necessary to prevent secondary cracking reactions and coke formation (*Zimmermann and Walzl, 2000*). A transverse-line heat exchanger (TLE) is used to cool the products to 250 °C, producing 320 °C high pressure saturated steam. To avoid tar fouling in heat exchangers (*Moulijn et al., 2013; Zimmermann and Walzl, 2000*), the products are subsequently water quenched to 25°C. A 'high pressure' (26 bar) C_2 splitter is implemented to better reflect industrial state-of-the-art operation. The drying unit is modeled as a flash column, where almost all of the water is condensed, and the acid gas removal (AGR) unit is placed at the exit of the compressor. A Sep block is used to simulate the AGR and PSA unit, with the energy consumption for each unit accounted for *(Ball, 2015; Fan, 2010; Rochelle, 2009)*. The solids

used in the simulation include Mn_3O_4 and MnO with MgO added as an inert to mimic the actual catalyst *(Neal et al., 2016*).

***Table S3a**: AspenPlus® modules, property methods and databanks* (Related to Figure 6 and Table 1)

Stream class	MIXCISLD
Databank	PURE, AQUEOUS, SOLIDS, INORGANIC
Solid components	Mn_3O_4, MnO, MgO
Property method	PR-BM and STEAM –TA for steam cycles
Unit operation models	
Regenerator, Reducer and De-acetylenizer	RStoic
Pressure changers	MCompr
Heat exchangers	Heater
Distillation columns	DSTWU
Separators/Flash columns	Sep/Flash2
Radiant zone of furnace	RGibbs
Convective zone of furnace	MHeatX

***Table S3b**: Simulation assumptions*

Ambient condition	T = 25°C, P = 1 atm
Reaction assumptions	As per the carbon yield distribution in Table S5 (below)
Heat loss in chemical looping reactors	1% of the total thermal output
Chemical looping reactor operating pressure	1 atm
Compressor specifications	4 stage with intercooler at 25°C Isentropic efficiency of 0.72
Air feed (to the regenerator)	10% excess
Discharge temperatures to the environment	Temperature: 25°C
Thermal energy to steam efficiency	85%
Thermal energy to electric energy efficiency	40%

***Table S4**: Operating conditions of the separation columns* (Related to Figure 6 and Table 1)

Unit	**Key component recoveries**				**Pressure (bar)**		**Condenser specifications**
	Light key	**Recovery**	**Heavy key**	**Recovery**	**Condenser**	**Reboiler**	
Demethanizer	Methane	99.90%	Ethylene	0.50%	34	35	Partial with vapor distillate
Deethanizer	Ethylene	99.99%	Propane	0.10%	26	27	Total
Depropanizer	Propylene	99.99%	Iso-butylene	0.1%	10	11	Total
C2-splitter	Ethylene	99.99%	Ethane	0.06%	25	26	Total

Four cases have been considered in the study, as described below, with the output for each listed in *Table S5 and S6*. Steam cracking data is based on the experimental data published in *(Froment et al., 1976;*

Sundaram and Froment, 1977), which were obtained in a pilot reactor for outlet total pressures of roughly 1 atm with negligible pressure drop and a steam dilution factor of 0.3-0.4 kg steam/kg feed ethane. The outlet temperature was 850^{o}C. Gas residence time of roughly 0.5 seconds was obtained under these conditions, which align well with the ones described in *(Moulijn et al., 2013; Sadrameli, 2015; Zimmermann and Walzl, 2000)*. ODH experiment conditions described thoroughly in the main document along with (*Neal et al., 2016; Yusuf et al., 2017)*, are in close agreement with those of steam cracking, for which the product distribution has been mentioned.

- *Steam cracking*

  Output is the typical steam cracking furnace product distribution based, on published data *(Froment et al., 1976; Sundaram and Froment, 1977; Zimmermann and Walzl, 2000)*

- *ODH 67 and 85*

  Hydrocarbon and CO_x yields based upon experimental results of the alkali salt doped Mg_6MnO_8 systems *(Neal et al., 2016; Yusuf et al., 2017)*

- *ODH 99*

  Hypothetical upper-end case for ODH to explore the extent of advantages, obtained by extrapolating the data obtained for ODH 85

***Table S5**: Product yields (carbon basis) used for the steam cracking and the various ODH cases* (Related to Section 2.3 and Table 1)

Case	**Cracking**	**ODH**		
Component		**%C yield**		
Ethane conversion (%)	**65**	**67**	**85**	**99**
Methane	3.40%	3.80%	5.94%	6.83%
Ethane	35.00%	32.20%	13.92%	1.00%
Ethylene	56.10%	57.30%	65.05%	74.81%
Propane	0.10%	0.20%	0.16%	0.19%
Propylene	1.20%	1.20%	2.05%	2.36%
iso-butane	0.20%	0.06%	0.00%	0.00%
n-butane		0.20%	0.07%	0.08%
Propadiene		0.05%	0.04%	0.05%
Acetylene	0.50%	0.46%	1.04%	1.20%
trans-2-butene		0.12%	0.05%	0.06%
1-butene		0.17%	0.12%	0.14%
i-butylene	0.20%	0.08%	0.01%	0.01%
c-2-butene		0.13%	0.05%	0.05%
i-pentane		0.07%	0.00%	0.00%
n-pentane	0.60%	0.07%	0.01%	0.01%
1,3-butadiene	2.10%	2.20%	4.69%	5.39%
Methyl acetylene		0.10%	0.14%	0.16%
trans-2-pentene		0.08%	0.03%	0.04%
2-methyl-2-butene		0.04%	0.01%	0.01%
1-pentene		0.07%	0.02%	0.02%
c-2-pentene		0.06%	0.01%	0.01%
Pentadiene		0.05%	0.21%	0.49%
Cyclopentadiene		0.05%	0.21%	0.00%
Benzene	0.50%	0.05%	1.05%	1.21%
Toluene	0.10%	0.05%	1.05%	1.21%
CO	0.00%	0.70%	1.83%	2.10%
CO2	0.00%	0.50%	2.24%	2.58%

***Table S6**: Broad product distribution (vol. %) used for the steam cracking (steam dilution: 0.4 kg/kg feed) and the various ODH cases* (Related to Figure 6 and Table 1)

Component	Concentration (vol. %)			
	Cracking	ODH 67	ODH 85	ODH 99
Ethane	16.33	19.34	7.21	0.47
Methane	3.07	4.56	6.16	6.60
Acetylene	0.23	0.32	0.63	0.68
Ethylene	26.10	34.35	33.71	36.15
Propylene	0.37	0.48	0.71	0.76
Propane	0.03	0.08	0.06	0.06
Butadiene	0.49	0.66	1.22	1.30
Butenes	0.05	0.15	0.06	0.06
Butanes	0.05	0.08	0.02	0.02
Pentane	0.11	0.09	0.10	0.11
Benzene	0.08	0.01	0.18	0.19
Toluene	0.01	0.01	0.16	0.17
Carbon monoxide	0.00	0.84	1.90	2.03
Carbon dioxide	0.00	0.60	2.32	2.49
Hydrogen	27.93	9.39	11.13	11.99
Water	25.14	28.99	34.37	36.83
Methyl acetylene	0.00	0.04	0.05	0.05
Propadiene	0.00	0.02	0.01	0.02
% H_2 combusted	NA	76		

The results obtained from the simulation are listed in *Table S7*. HVP represents the High Value Products. Energy for CO_2 removal was assumed to be *0.11 MW-hr/tonne CO_2 removed (Fan, 2010; Rochelle, 2009).* For H_2 purification, only the amount required for acetylene hydrogenation has been separated; using Pressure Swing Adsorption (PSA): *2.2 kW-hr/kg H_2 (Ball, 2015).*

***Table S7**: Unit-wise distribution of energy demand for all the cases* (Related to Section 2.3 and Table 1)

Unit	Cracking	ODH 67	ODH 85	ODH 99
Energy Consumed (GJ)/Tonne HVP	**0.91**	**0.91**	**0.86**	**0.86**
Reactor/Furnace	6.63	0.00	0.00	0.00
Regenerator	0.00	0.00	-1.30	-1.42
Feed and recycle treatment	9.67	3.20	2.55	2.20
Quench	-3.92	-3.38	-2.93	-2.60
Compressor	3.31	2.32	2.04	1.87
Refrigeration steps	2.37	1.63	1.31	1.15
Demethanizer	0.22	0.24	0.23	0.23
De-ethanizer	1.29	1.26	0.94	0.79
C2-splitter	1.53	1.48	1.22	1.22
Depropanizer	0.04	0.02	0.05	0.04
Deacetylenizer	0.00	0.90	0.87	0.69
CO_2 removal	0	0.02	0.09	0.09
H_2 purification	0	0.01	0.02	0.02
Total	**21.13**	**7.69**	**5.09**	**4.27**

Exergy analysis (Querol et al., 2013; Rivero and Garfias, 2006; Szargut, 1989)

Total exergy = Physical exergy + Chemical exergy

- **<u>Physical exergy</u>**, $b_{ph} = (h-h_o)-T_o(s-s_o)$

Quantity X_o stands for the value at the reference state, which is T_o =298.15K and P_o=1 atm

- **<u>Chemical exergy</u>**: The environment is the dead (reference) state

***Table S8**: Chemical exergy of the compounds at reference state* (Related to Section 2.4 and Table 2)

	X_{ref}(mole fraction)	b_{chem}(kJ/mole)	G (kJ/mole)
N_2	0.765	0.7	0
O_2	0.206	3.9	0
CO_2	0.0003	20.1	-394.4
H_2O	0.019	1.3	-237.1
%RH	60		

For 1 mole $C_xH_yO_z$: $x.\ CO_2 + a.\ H_2O = C_xH_yO_z + c.\ O_2$

- $b_{chem(CxHyOz)} = x.\ b_{chem(CO2)} + a.\ b_{chem(H2O)} + \Delta G_{(CxHyOz)} - c.\ b_{chem(O2)}$
- For change in concentration of reference compounds, subtract the term*: -R.T.ln (xi or RH)* from the reference value

***Table S9**: Calculated chemical exergy of the various compounds* (Related to Section 2.4 and Table 2)

Compound	Formula	ΔG (kJ/mol)	b (kJ/mol)
Ethane	C_2H_6	1467	1497.5
Methane	CH_4	818	832.7
Acetylene	C_2H_2	1235	1266.8
Ethylene	C_2H_4	1094	1125.8
Propylene	C_3H_6	1969	2015.8
Propane	C_3H_8	2108	2154.2
Butadiene	C_4H_6	2441	2503.6
Butenes	C_4H_8	2592	2654.1
Butanes	C_4H_{10}	2749	2810.1
Pentane	C_5H_{12}	3386	3462.4
Benzene	C_6H_6	3202	3297.4
Toluene	C_7H_8	3820	3930.5
Carbon monoxide	CO	257	275.3
Carbon dioxide	CO_2	394	20.1
Hydrogen	H_2	237	236.4
Water	H_2O	237	1.3
Methyl acetylene	C_3H_4	1856	1902.8
Propadiene	C_3H_4	1856	1902.8
Oxygen	O_2	0	3.9
Nitrogen	N_2	0	0.7
Nitric oxide	NO	181	182.8
Nitrogen dioxide	NO_2	66	70.6

Sample exergy calculations

Chemical exergy

Using the values given in *Table S8* and ΔG from *S9,* consider the compound ethane (C_2H_6). For 1 mole C_2H_6: $2\ .CO_2 + 3.\ H_2O = C_2H_6 + 3.5\ O_2$

- $b_{chem(C2H6)} = 2.\ b_{chem(CO2)} + 3.\ b_{chem(H2O)} + \Delta G_{(C2H6)} - 3.5.\ b_{chem(O2)}$
- $b_{chem(C2H6)} = 2.\ (20.1) + 3.\ (1.3) + 1467 - 3.5.\ (3.9) =$ ***1497.5 kJ/mol***

Consider the compound carbon monoxide (CO). For 1 mole C_2H_6: $CO_2 = CO + 0.5\ O_2$

- $b_{chem(CO)} = b_{chem(CO2)} + \Delta G_{(C2H6)} - 0.5.\ b_{chem(O2)}$
- $b_{chem(C2H6)} = 20.1 + 257 - 0.5.\ (3.9) =$ ***275.3 kJ/mol***

- With the calculated chemical exergy of each component, the chemical exergy component of each process stream can be obtained, which along with the physical component, provides the total exergy (of the stream). This is demonstrated in the idealized exergy flow diagram in *Figure 3 (of main text)*.
- With the exergy (or exergy flow in GJ/hr) obtained for each process stream, the exergy loss across each unit can be calculated. It can be normalized per tonne of ethylene product or HVP

Exergy loss (across each unit) = Lost work (GJ/tonne HVP) = Exergy in – Exergy out

- With the exergy loss across each unit, the overall exergy loss for the entire process can be calculated and compared with different process schemes

$$\textit{Exergy loss (entire process)} = \sum_{\textit{(all units)}} \textit{Exergy loss across each unit}$$

Physical exergy

Consider a stream of pure ethane, which has a chemical exergy of 1497.5 kJ/mol as described earlier. *Figure S6* shows the change in physical exergy (and total exergy) of the stream with a change in temperature (at 1 atm), which is calculated using the databanks in AspenPlus®. Using a similar method, the exergy loss across each unit is calculated for the processes, which is listed in *Table S10*. The comparison of the cases is depicted in *Figure S7*.

***Table S10**: Exergy losses (GJ/tonne HVP) calculated using AspenPlus® functions (excluding chemical exergy)* (Related to Section 2.4 and Table 2)

Separation Unit	Cracking	ODH 67	ODH 85	ODH 99
CO2 scrub	0.000	0.010	0.032	0.034
De-acetylenizer	0.101	0.167	0.189	0.149
PSA	0.000	0.005	0.005	0.008
Demethanizer	0.286	0.296	0.249	0.225
De-ethanizer	0.512	0.493	0.370	0.314
C2-splitter	0.612	0.640	0.488	0.487
Depropanizer	0.015	0.007	0.022	0.017
Total separation	**1.526**	**1.618**	**1.355**	**1.233**

Power Generation Block

The approach in *Figure S8*, based on *(Siva Reddy et al., 2014)*, was utilized while calculating the exergy losses in the power generation block as shown in *Figure 6 (of main text)*.

CO_2 emissions

Results obtained using the different assumptions, to compare the CO_2 emissions, are presented in *Table S11* and *Figure S9*.

***Table S11**: CO_2 emissions using the various assumptions (as depicted in Figure 7)* (Related to Section 2.5, Figure 7 and Table 3)

	Steam Cracking	ODH 67	ODH 85	ODH 99
No H_2 Credit	1.256	0.475	0.355	0.306
Mixed Fuel Gas	0.689	0.332	0.265	0.238
with H_2 Credit	0.635	0.318	0.177	0.131
CO_2 Capture Credit	0.635	0.292	0.084	0.038

Available and imported fuel

In *Figure S10*, all the H_2 has been purified and separated via PSA. Available CO and CH_4 are assumed to be combusted first, with 100% efficiency. The remaining demand is met by importing CH_4.

References

Ball, M. (2015). Compendium of hydrogen energy, volume 4: hydrogen use, safety and the hydrogen economy, 1st edition. ed, Woodhead Publishing Series in Energy 4. Elsevier, Waltham, MA.

Fan, L.-S. (2010). Chemical looping systems for fossil energy conversions. Wiley-AIChE, Hoboken, NJ.

Froment, G.P., Van de Steene, B.O., Van Damme, P.S., Narayanan, S., Goossens, A.G. (1976). Thermal Cracking of Ethane and Ethane-Propane Mixtures. Ind. Eng. Chem. Process Des. Dev. 15, 495–504

Haribal, V.P., Neal, L.M., Li, F. (2017). Oxidative dehydrogenation of ethane under a cyclic redox scheme – Process simulations and analysis. Energy 119, 1024–1035.

Moulijn, J.A., Diepen, A. van, Makkee, M. (2013). Chemical process technology, Second edition. ed. John Wiley & Sons Inc., Chichester, West Sussex, United Kingdom.

Neal, L.M., Yusuf, S., Sofranko, J.A., Li, F. (2016). Oxidative Dehydrogenation of Ethane: A Chemical Looping Approach. Energy Technol. 4, 1200–1208.

Querol, E., Gonzalez-Regueral, B., Perez-Benedito, J.L. (2013). Exergy Concept and Determination, in: Practical Approach to Exergy and Thermoeconomic Analyses of Industrial Processes. Springer London, London, pp. 9–28.

Rivero, R., Garfias, M. (2006). Standard chemical exergy of elements updated. Energy 31, 3310–3326.

Rochelle, G.T. (2009). Amine Scrubbing for CO2 Capture. Science 325, 1652–1654.

Sadrameli, S.M. (2015). Thermal/catalytic cracking of hydrocarbons for the production of olefins: A state-of-the-art review I: Thermal cracking review. Fuel 140, 102–115.

Siva Reddy, V., Kaushik, S.C., Tyagi, S.K. (2014). Exergetic analysis and evaluation of coal-fired supercritical thermal power plant and natural gas-fired combined cycle power plant. Clean Technol. Environ. Policy 16, 489–499.

Sofranko, J.A., Li, F., Neal, L. (2016). Oxygen transfer agents for the oxidative dehydrogenation of hydrocarbons and systems and processes using the same. WO2016049144A1.

Sundaram, K.M., Froment, G.F. (1977). Modeling of thermal cracking kinetics—I. Chem. Eng. Sci. 32, 601–608.

Szargut, J. (1989). Chemical exergies of the elements. Appl. Energy 32, 269–286.

Yusuf, S., Neal, L.M., Li, F. (2017). Effect of Promoters on Manganese-Containing Mixed Metal Oxides for Oxidative Dehydrogenation of Ethane via a Cyclic Redox Scheme. ACS Catal. 7, 5163–5173.

Zimmermann, H., Walzl, R. (2000). Ethylene, in: Ullmann's Encyclopedia of Industrial Chemistry.Wiley-VCH Verlag GmbH & Co. KGaA.